HAL
open science

Mode I cohesive zone model parameters identification and comparison of measurement techniques based on uncertainty estimation

Agathe Jaillon, Julien Jumel, Frederic Lachaud, Eric Paroissien

To cite this version:

Agathe Jaillon, Julien Jumel, Frederic Lachaud, Eric Paroissien. Mode I cohesive zone model parameters identification and comparison of measurement techniques based on uncertainty estimation. International Journal of Solids and Structures, 2020, 191-192, pp.577-587. 10.1016/j.ijsolstr.2019.12.014 . hal-02549254

HAL Id: hal-02549254

https://hal.science/hal-02549254

Submitted on 21 Apr 2020

HAL is a multi-disciplinary open access archive for the deposit and dissemination of scientific research documents, whether they are published or not. The documents may come from teaching and research institutions in France or abroad, or from public or private research centers.

L'archive ouverte pluridisciplinaire **HAL**, est destinée au dépôt et à la diffusion de documents scientifiques de niveau recherche, publiés ou non, émanant des établissements d'enseignement et de recherche français ou étrangers, des laboratoires publics ou privés.

Open Archive Toulouse Archive Ouverte (OATAO)

OATAO is an open access repository that collects the work of some Toulouse researchers and makes it freely available over the web where possible.

This is an author's version published in: https://oatao.univ-toulouse.fr/25253

Official URL: https://doi.org/10.1016/j.ijsolstr.2019.12.014

To cite this version :

Jaillon, Agathe and Jumel, Julien and Lachaud, Frédéric and Paroissien, Eric Mode I Cohesive Zone Model Parameters Identification and Comparison of Measurement Techniques based on uncertainty estimation. (2020) International Journal of Solids and Structures, 191-192. 577-587. ISSN 0020-7683

Any correspondence concerning this service should be sent to the repository administrator:
tech-oatao@listes-diff.inp-toulouse.fr

Mode I Cohesive Zone Model Parameters Identification and Comparison of Measurement Techniques based on uncertainty estimation.

Agathe Jaillon[a], Julien Jumel[b], Frédéric Lachaud[a], Eric Paroissien[a]

a: Institut Clément Ader (ICA), Université de Toulouse, CNRS-INSA-ISAE-Mines Albi-UPS, UMR 53123 Rue Caroline Aigle, F-31400 Toulouse

b: I2M, Université de. Bordeaux, Arts et Métiers Paris Tech, CNRS, I2M, UMR 5295, F-33400 Talence

Abstract

Adhesive bondline mechanical behaviour is frequently described with cohesive zone models (CZM). For mode I loading condition these phenomenological laws simply represent the evolution of the peel stress as a function of the two adherends relative displacement normal to the joint. Generally, these laws are identified rather than really measured using experimental data obtained from crack initiation and propagation experiments such as the Double Cantilever Beam Test (DCB). The uncertainty on parameter estimation are generally not indicated, as for a DCB test it is only the critical energy release rate that has the most influence on the results. However, the uncertainties on the other parameters prevent the use of the identified TSL for other mechanical tests where mode I solicitations are predominant. In this article, the purpose is to evaluate the methodologies reliability for the assessment of mode I CZM. To do so, several methods used to evaluate CZM parameters are compared in terms parameter estimation reliability. Synthetic noisy data are considered for a χ^2 function minimisation. Then, sensitivity calculations are performed to determine the estimated parameters standard deviation. By applying this procedure on different type of synthetic measurements (respectively $P(\Delta)$, $J(\delta,\theta)$, backface strain and DIC) the ability of these different techniques to capture the best parameters for a chosen CZM shape can be rigorously evaluated.

Keywords: DCB; Cohesive zone model; Chi-square; sensitivity; confidence interval; comparative study; DIC

Nomenclature

a	=	Parameters vector
a_0	=	Initial crack tip length (mm)
C	=	Covariance matrix
$corr$	=	Correlation matrix
Δ	=	Opening at loading point (mm)
δ	=	Opening at crack tip (mm)
ε_s	=	Adherend deformation measured by gauges (μdef)
E	=	Young's modulus of the adherend(MPa)
E_a	=	Young's modulus of the adhesive (MPa)
G_a	=	Shear modulus of the adhesive (MPa)
G_c	=	Critical energy release rate (N/mm)
I	=	Quadratic moment (m^4)
J	=	Integral J (N/mm)
k	=	Parameters' index number
L	=	Bonded overlap length (mm)
n_d	=	Number of measured data
n_p	=	Number of parameters
P	=	Force (N)
σ	=	Stress in the adhesive (MPa)
σ_{max}	=	CZM Maximal stress (MPa)
σ_{noise}	=	Gaussian noise standard deviation
σ_Y	=	Standard deviation
S	=	Sensitivity function

θ	=	Rotation at loading point (rad)
t	=	Adherend thickness (mm)
t_a	=	Adhesive bond thickness (mm)
t_i	=	Data index number
v_p	=	Displacement jump at propagation (μm)
w	=	adherend width (mm)
χ^2	=	Chi square function
x	=	abscissa along the overlap (mm)
Y	=	Experimental data vector
$\hat{Y}$	=	Theoretical data vector
Y_0	=	Area under the TSL elastic part (N/mm)

Abbreviations

CI		Confidence Interval
CZM		Cohesive zone model
DCB		Double cantilever beam
DIC		Digital image correlation
FE		Finite Element
Std		Standard deviation
TS	=	Traction separation
TSL	=	Traction separation law

1 Introduction

Adhesive bonding has gained growing interest in many fields in particular in the transportation industry. Indeed, this joining technique is known to offer a very competitive strength to mass ratio. It is very adequate for composite structure assembly and leads to drastic reduction of the fasteners numbers. However, the reliability of bonded joints is difficult to assess especially in the aeronautical sector where the certification procedure for structural parts are very demanding. The variability on the bonded joint strength may be due to strong sensitivity to any surface pollution, or uncontrolled ageing phenomena but is also a consequence of inadequate mechanical testing protocols. Indeed, the bonded interface behaviour is still mainly determined with standard procedure, the tensile test on single lap joint specimen being the most common one. The test results are known to be dependent on the test conditions such as the loading rate, but also on the specimen geometry (adherend and adhesive thicknesses, overlap length) and not only on the interface properties.

These past years Cohesive Zone Model (CZM) were introduced to describe the interface behaviour and simulate the joint behaviour. These phenomenological laws have been also used to simulate delamination processes in laminates. They represent the cohesive stresses versus interface relative displacement evolution and could be considered as more robust models since they describe not only the interface elastic behaviour but also irreversible phenomena such as damage and/or plasticity. They enable a refined evaluation of the cohesive stresses distribution along the interface during monotonous loading of the joint.

These models have been studied extensively from a theoretical and numerical point of view and many contributions have used them for failure load prediction of many different materials [1] [2] [3]. Considering pure mode I loading condition, these models are alternatively called traction separation laws (TSL). Their shapes and corresponding parameters are usually empirically chosen according to the expected material global

behaviour (i.e. brittle, ductile). TS parameters are adjusted using iterative procedure so that a good agreement is found between experimental data and theoretical value found with an analytical [4] or numerical model [5] [6]. The data used for the identification are generally simple applied load versus resulting displacement even if more sophisticated technique are also described.

The use of CZM should improve the joint strength prediction through more precise description of the interface mechanical behaviour. However, the prediction of both crack initiation and propagation regime may still suffer from a lack of precision mainly because the TSL shape is chosen empirically rather than really being measured. Previous contributions have evidenced that the predicted mechanical response of the joint depends on the TSL shape especially for ductile adhesives [7] [8] [9]. This is why an extensive work has been ongoing for the development of specialized experimental techniques for measuring precisely the interface separation law (i.e. cohesive stress versus displacement jump across the interface). These new characterization protocols lead to the use of new specimen and loading systems such as the DCB fixture developed by Sørensen et al. which enable the direct determination of the TSL through the differentiation of the J-integral [10] [11]. This same technic is used by Anderson et al. but the adhesive elongation is measured with interference patterns [12]. The development of digital image correlation over the last decades has also given access to a whole new range of mechanical response. As it is possible to monitor the adherends' deflection and rotation throughout the entire test. Shen and Paulino then used a hybrid inverse method based on finite element analysis and Digital Image Correlation (DIC) to determine the TSL shape and associated parameters [13]. DIC was also used by Lelias et al as a direct method to extract the CZM using the differentiation of displacement and rotation at crack tip [14]. More systematic routine to identify CZM from DCB test with digital image correlation monitoring has been proposed by Alfano et al. [15] and Blaysat et al. [16]. Adherends'

deformation can also be measured using optical [17] or resistive [18] strain gauges. As it enable a precise location of the crack tip but can also be used for the direct identification of the CZM through the differentiation of the backface strain signal evolution [19]. Direct inversion techniques have also been proposed for the CZM reconstruction from the experimental data obtain with BSM and J(θ) techniques. On the contrary inverse methods should be used to analyse DIC and P(Δ) measurements [14]. In these cases, some assumptions are made on the TSL shape which must be set arbitrary and which can lead to errors on latter predictions [20]. Moreover, the incorrect estimation of the TSL parameters can also lead to erroneous prediction when applied to other kind of mechanical tests that are subjected to mode I or more complex solicitations (i.e. SLJ, DLJ, …).

Then, this contribution aims at proposing a systematic procedure to evaluate the sensitivity of the four methods ($P(\Delta)$, DIC, $J(\theta,\delta)$, BSM) to evaluate a triangular TSL parameters such as interface stiffness, strength and fracture energy. A simple semi-analytical model of a DCB experiment considering non-linear interface behaviour is used to generate synthetic experimental data with known interface behaviour. Some Gaussian noise [21] is added to the data then a Levenberg-Marquart algorithm is used to minimize an error function and identify the triangular TSL parameters. The Confidence domains for the group of fitted parameters are obtained at the end of the minimization procedure for all four measurement-techniques. They can be used for the evaluation of the identification quality and the techniques' comparison.

2 χ^2 minimisation and confidence intervals theoretical background

Obtaining model parameters from a set of experimental data can be achieved with different techniques. The most common technique consists in minimizing an error function which may exhibit significantly non-linear behaviour. In the following, least square minimization is realised considering the Chi square, χ^2, function defined with relation :

$$\chi^2(a) = \sum_{t_i=1}^{n_d} \left[\frac{Y(t_i) - \hat{Y}(a, t_i)}{\sigma_Y(t_i)} \right]^2 \qquad \text{(eq 1)}$$

In equation (eq 1) Y(t_i), t_i={1,…, n_d} represent the n_d measured data used to identify the a_k k={1,…,p} parameters. $\hat{Y}$ are the corresponding theoretical data obtained with the model. In equation (eq 1), the terms in the sum are weighted by the measurement error on the experimental data σ_Y. This function is minimized using steepest gradient technique such as Levenberg-Marquart algorithm until the minimum χ^2value is found and the corresponding optimum set of parameters is determined. The quality of the optimization process can then be evaluated using the R^2-*value*.

Once a, the optimal parameters' vector is found, parameters confidence intervals can be evaluated by analysing the χ^2 function evolution near the minima. Indeed, the small variation of one or several parameters will lead to an increase of the χ^2 value, a steep increase meaning a high sensibility to any parameter fluctuation and then high reliability of the identification process. First, evaluation of the confidence interval is obtained by performing second order Taylor expansion of the χ^2 function near the minima. This results in a simple quadratic approximation of the error function given by:

$$\Delta\chi^2 = \delta a \, C^{-1} \delta a \qquad \text{(eq 2)}$$

Where the covariance matrix is defined as

$$C = {\sigma_Y}^2 (SS^T)^{-1} \qquad \text{(eq 3)}$$

with S corresponding to sensitivity function:

$$S = [S_k(t_i)] = \frac{\partial \hat{Y}(a, t_i)}{\partial a_k} \qquad \text{(eq 4)}$$

Assuming the standard deviation, ${\sigma_Y}^2$, is constant for all data points (eq 5), it can be estimated with the equation [22]:

$$\sigma_Y{}^2 = \frac{\sum_{t_i=1}^{n_d}\left(Y(t_i) - \hat{Y}(p, t_i)\right)^2}{n_d - n_p} \qquad i \in [1{:}\, n_d] \qquad \text{(eq 5)}$$

The confidence intervals on the identified parameters can be obtained from the analysis of the χ^2 function evolution near the minimum. Indeed, for a given reliability and number of degree of freedom (n_d - identified parameters) the variation $\Delta\chi^2$ of the error function due to parameters variation δa should be less than the value defined by χ^2 function values table. From the asymptotic analysis and expression, these confidence intervals can be estimated once the covariance matrix has been determined. The envelope of the confidence domain is then represented by an ellipsoid, when three parameters are identified. Likewise, for two parameters it is represented as an ellipse. However, the real shape of the confidence region might be different if the minimization problem is highly nonlinear.

For visualisation and analysis purposes, it might be needed to reduce the number of parameters used. As joint confidence regions are larger than individual intervals for the same confidence. It is then possible to project the covariance matrix on a lesser dimension.

The confidence region analysis can also give information on the correlation of the parameters. A correlation matrix can be determined using the covariance matrix [23]. It will give access to a normalised estimation of the linear correlation between each pair of parameters, diagonal parameters being equal to one.

$$corr(i.j) = \frac{C(i,j)}{\sqrt{C(i,i)}\sqrt{C(j,j)}} \qquad (i,j) \in \left[1{:}\, n_p\right] \qquad \text{(eq 6)}$$

Knowing the correlation between parameters is important as it gives indication on how uncertainties on one parameter propagate to another.

3 DCB mechanical response

Parameter estimation and confidence regions determination for a model require numerous model calculation that can become quite time costly. In order to avoid too much calculation time, it appeared wiser to implement an analytical model rather than using finite element (FE) model. The purpose of this analytical model is to simulate the mechanical response that could be measured during an experimental DCB test. That is to say that it needs to give access to all the specimen mechanical response enabling the determination of the load, the opening at loading point, the rotation at loading point, the adherends' deformation along the overlap and the adherends' rotation along the overlap. These responses can be determined with the mechanical fields computed during the crack propagation along the overlap for an adhesive having a bilinear CZM.

3.1 Modelling of DCB test with nonlinear interface behaviour

The DCB specimen, illustrated in Figure 1, is modelled as two Timoshenko beams having rectangular cross section (width: *w*, thickness: *t*) and bonded with an adhesive layer whose TS behaviour is represented with a bilinear TSL. The length of the bonded part is *L*. On the right end of the specimen the two slabs are left unbounded over a distance equal to a_0 and considered as the initial crack length.

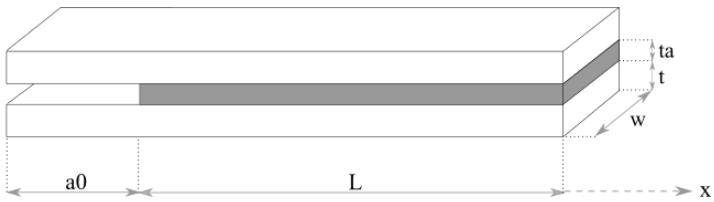

Figure 1: DCB specimen geometric data considered in the analytical model

The solving the local beam equilibrium enables the determination of the load displacement and $J(\theta,\delta)$ curves during the whole test, as well as the shear forces, bending moment, adherends deflection and along the overlap. The whole analytical resolution methodology is detailed in Jaillon et al. [20].

3.2 Indirect traction-separation law identification techniques.

To illustrate the need for TSL identification techniques, some DCB test simulations are carried out for three bilinear TSLs. The DCB test specimen characteristics are presented below considering triangular TSL which are defined by the adhesive effective modulus E_a, the maximum stress σ_{max}, and the critical energy release rate G_c. The chosen values are summed up in Table 1.

Table 1: Traction separation laws parameters

Reference	$\boldsymbol{E_a}$ **(MPa)**	$\boldsymbol{\sigma_{max}}$ **(MPa)**	$\boldsymbol{G_c}$ (N/mm)
TS1	146	14	1.4178
TS2	20	11	1.4178
TS3	300	20	1.4178

These TSL can be displayed as stress function of displacement jump at crack tip, as Figure 2 illustrates it. In order to emphasize the importance of the TSL on the bonded specimen mechanical response, these three laws will be used to compare the mechanical fields obtained for each measurement method commonly used for DCB tests. Moreover, as this test is most sensitive to the value of the critical energy rate, all three examples have the same one in order to better visualize the differences due to the TSL parameters' value only.

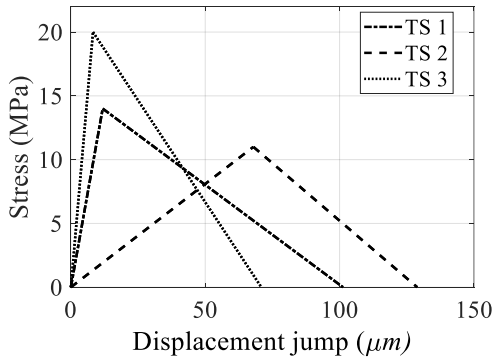

Figure 2: Three bilinear TSL.

3.2.1 TSL identification from the P(Δ) measurement technique

The first method proposed to evaluate TSL from DCB experiment is based on the analysis of the force, *P*, versus opening displacement evolution, *Δ*. Since the original analysis of DCB

test [24], these data are systematically measured as it enables the evaluation of the interface critical energy release rate which is based on compliance measurement evolution. As it can be seen on Figure 3(a), *P(Δ)* curve is typically composed of three parts corresponding to the CZM. The first one is linear. Then, once the adhesive begins to soften, the force keeps increasing but nonlinearly and finally, when the critical energy release rate is reached crack propagation begins.

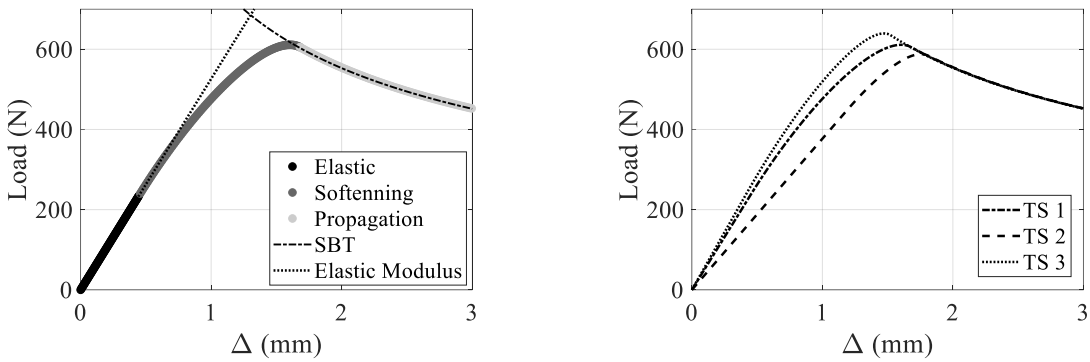

(a) (b)

Figure 3: Load-displacement curves: (a) Division of the P(Δ) curve according to the TSL phase; (b) Impact of the TSL on the P(Δ) response.

The responses from the three TSLs are presented in Figure 3(b) showing how the TSL may affect the overall response of the specimen during testing. The TSL has an impact on the phases previous to the crack propagation and it appears that it will affect the maximum force, the opening displacement at crack propagation beginning and the nonlinearity of the peak. Moreover, when the modulus is high, its impact become less significant and can be concealed by the measurement noise.

3.2.2 TSL identification from the J(θ,δ) measurement technique

The J integral evolution during the DCB test is obtained directly by measuring the specimen end rotation together with the applied load [25] [26]. The *J(θ,δ)* evolution reduces to three different regions, the elastic ad softening ones showing parabolic evolutions but with opposite curvature and the third one being constant when J remains stationary as crack

propagation begins (Figure 4(a)). It appears that the TSL has an impact on the curvature of the parabolas (Figure 4(b)). It also influences the opening value for which the energy release rate becomes constant.

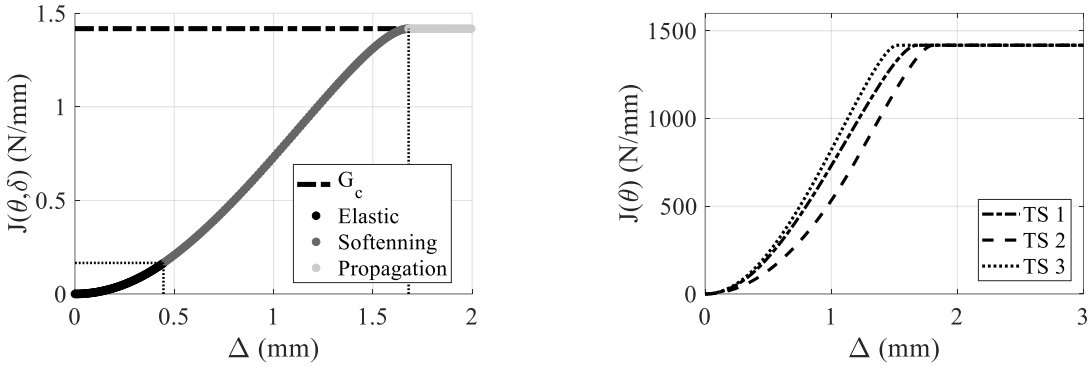

(a) (b)

Figure 4: Integral J function of the opening at loading point: (a) Division of the *J(θ,δ)* curve according to the TSL phase; (b) Impact of the TSL on the *J(θ,δ)* response.

3.2.3 TSL identification from the Backface Strain measurement technique

Resistive gauges can be placed on the adherend's upper face. The measurement of the slabs deformation, ε_s, gives insight on the stress state of the adhesive bond directly underneath the gauges using the relation:

$$\sigma = -2\frac{EI}{wt}\frac{\partial^2 \varepsilon_s}{\partial x^2} \qquad \text{(eq 7)}$$

The gauges response is an indicator of the stress state of the adhesive below which phases are given by Figure 5(a). It is worth noticing that the adherend deformation is maximal when the crack tip is close to the gauge and that its value and curvature is influenced by the TSL as illustrated in Figure 5(b).

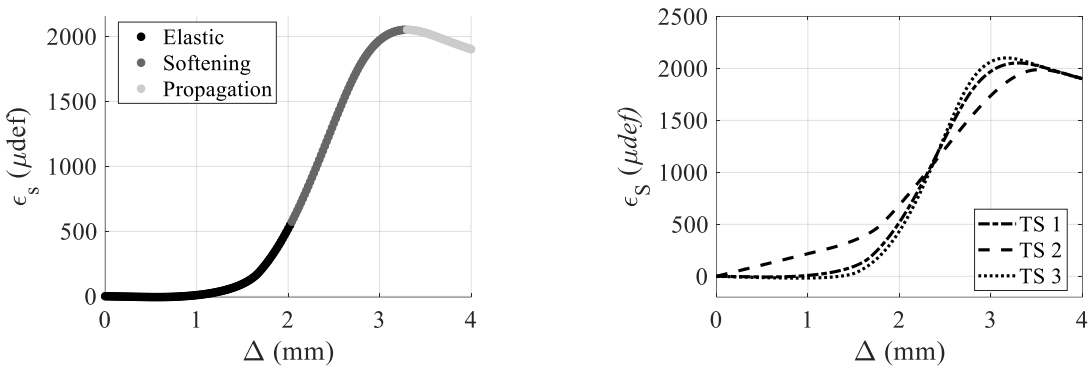

(a) (b)

Figure 5: Gauges deformation function of the opening at loading point: (a) Division of the Gauge curve according to the TSL phase; (b) Impact of the TSL on the Gauge response.

3.2.4 TSL identification from DIC measurement technique

During a DCB test digital image correlation (DIC) can be used to determine the deflection and rotation of the adherends along the bonded area. Experimentally, this requires the use of a speckle pattern and one or a couple of cameras. In the analytical model, the adherends deflection and rotation of the neutral fibre are directly computed along the specimen without generating any images of the adherends side. Moreover, in order to only investigate the behaviour of the adhesive, the deflection and rotation of the adherend are analysed from the crack tip abscissa $X = -50$ *mm* to $X = 120$ *mm*. The test is also only considered for an opening at loading point included between $\Delta = 1$ *mm* and $\Delta = 2$ *mm*. Figure 6(a and b) highlights the adhesive behaviour according to the CZM phase. It also enables the visualization of the crack advances. The influence of the TSL is illustrated by Figure 6(c and d) for the deflection and rotation of the adherends for $\Delta = 1$ *mm*. The impact seems to be negligible and the differences are likely to be concealed by experimental noise.

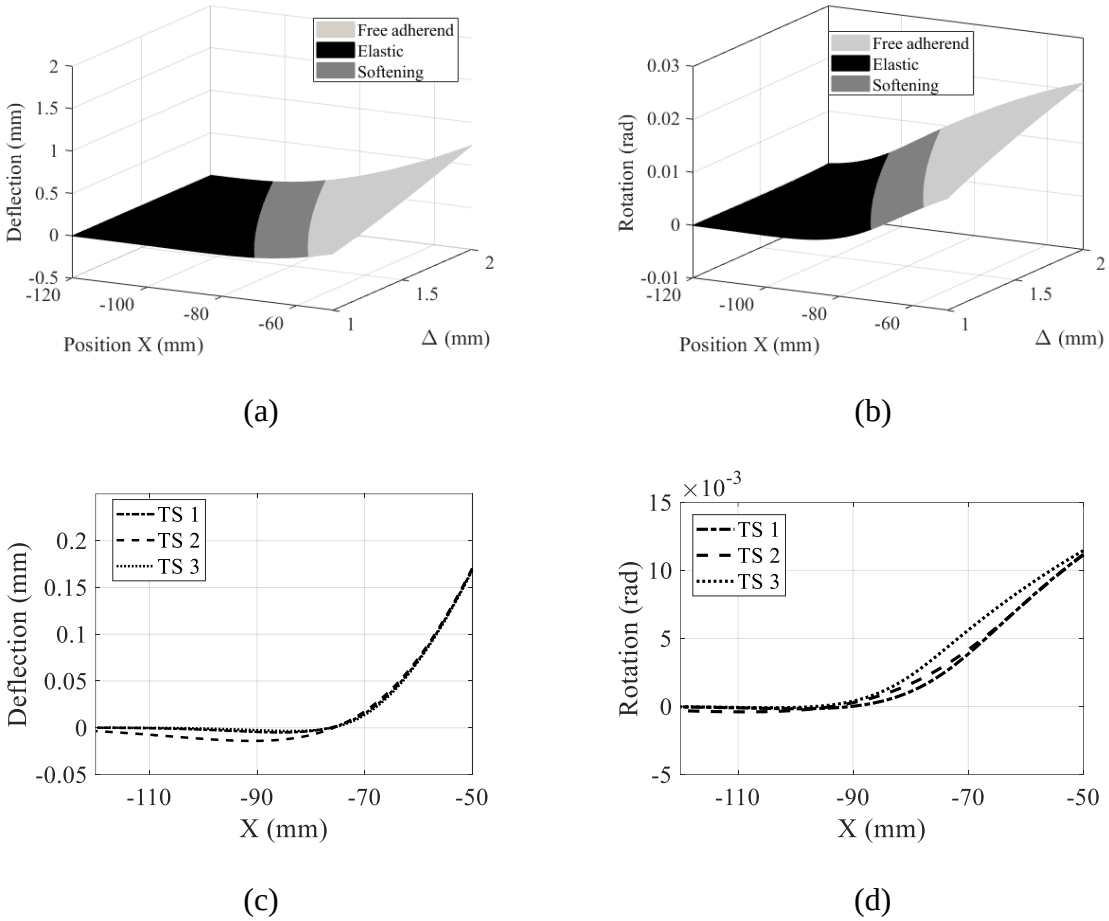

Figure 6: Digital image correlation results along the overlap during a DCB test: (a) Division of the DIC – deflection curve according to the TSL phase; (b) Division of the DIC – rotation curve according to the TSL phase; (c) Impact of the TSL on the deflection response; (d) Impact of the TSL on the rotation response;

4 Confidence regions identification methodology

4.1 Material and geometric parameters

The analytic model, presented earlier, is used to simulate a DCB specimen. Its geometric and material characteristics are summarized in Table 2. The adhesive, whose thickness is chosen at 247µm, is implemented using a triangular cohesive zone model whose chosen parameters of interests are arbitrarily chosen: the initial modulus the maximum stress and the displacement jump at propagation: $a = [E_a, \sigma_{max}, v_p]$. Table 2 includes the chosen nominal

parameters and the associated critical energy release rate in mode I and surface area under the elastic part, respectively G_c and Y_0.

Table 2: DCB specimen geometric and material characteristics

Adherends		**Adhesive TSL**	
Total length (mm)	180	E_a (MPa)	146
Overlap length (mm)	130	σ_{max}(MPa)	14
Initial crack length (mm)	50	v_p(µm)	101.27
Thickness (mm)	10	Y_0 (N/mm)	0.67
Width (mm)	15	G_c (N/mm)	1.42
Young modulus (GPa)	70		
Poisson ratio (-)	0.3		

4.2 Synthetic experimental data generation

The analytical model is used to generate the nominal response of each mechanical field previously described. In order to carry out the inverse identification and to estimate the confidence intervals, a first approach is to generate synthetic experimental data by applying a Gaussian noise. This noise enables the representation of experimental uncertainties that are due to the measurement chain (i.e. load captors, gauges, DIC...). For each mechanical response, a custom noise is generated as a normal distribution whose mean is equal to zero and whose standard deviation is approximately 1% of the maximal mechanical response (Table 3). Figure 7 displays the associated experimental data and optimisation results.

Table 3: Applied noise mean value for each mechanical response.

Method	**P(Δ)**	**J(θ,δ)**	**Gauges**	**DIC - Deflection**	**DIC - Rotation**
Units	N	kJ/m²	µdef	mm	rad
$\boldsymbol{\sigma_{noise}}$	10	10	20	0.01	0.005

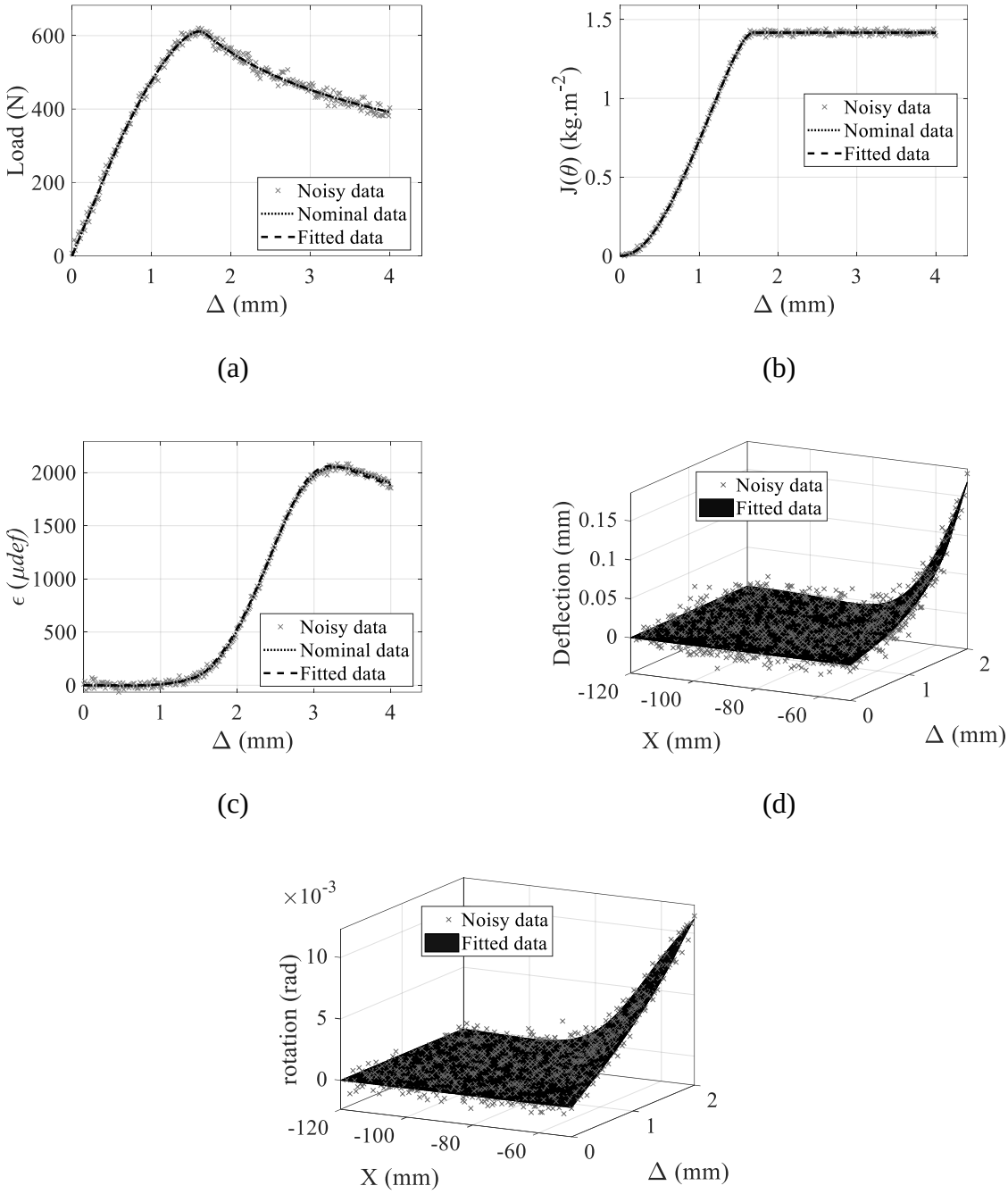

Figure 7: Synthetic measurements data with its optimization result; (a) P(Δ); (b) J(θ,δ); (c) Gauges; (d) DIC - deflection; (e) DIC – rotation.

The minimization and confidence interval identification procedure were carried out for each mechanical response that can be obtained on a DCB test. For clarity purpose, the process will only be detailed for the force-displacement curve as it is similar for the other methods.

4.3 Application to the Force-displacement curve

The χ^2 minimization is executed on experimental data in order to determine the optimized parameters triplet. To identify the confidence regions, sensitivity functions are determined analytically using equation (eq 4). Mechanical responses are computed for a ±5% variation of each parameters. The standard deviation (eq 5) between the optimized model data and the experimental data are then computed enabling the determination of the covariance matrix. It is possible to draw the confidence region in three-dimension, projected on 2-parameters plane and projected in 1 dimension which gives access to confidence regions and intervals. The confidence regions at 95% of the force-displacement curves are illustrated in Figure 8. The ellipsoid and ellipses are centred on the nominal value. As expected, the individual confidence intervals are smaller than the regions in two dimensions. It appears that the 95% confidence intervals (i.e. individual) for the modulus is comprised between 127.3MPa and 164.7 MPa, for the maximal stress between [13.7, 14.5] MPa and for the displacement jump between [98.2, 104.4] µm. Moreover, in order to assess the quality of the minimization and confidence regions, the χ^2 optimization has been carried out 12 times for experimental data on which were applied a new random noise. The results of these minimizations are illustrated in Figure 8 as grey diamonds. It can be noticed that they are all included in the confidence regions and intervals which is a quality assurance of the minimization procedure and shows that the results are reproducible.

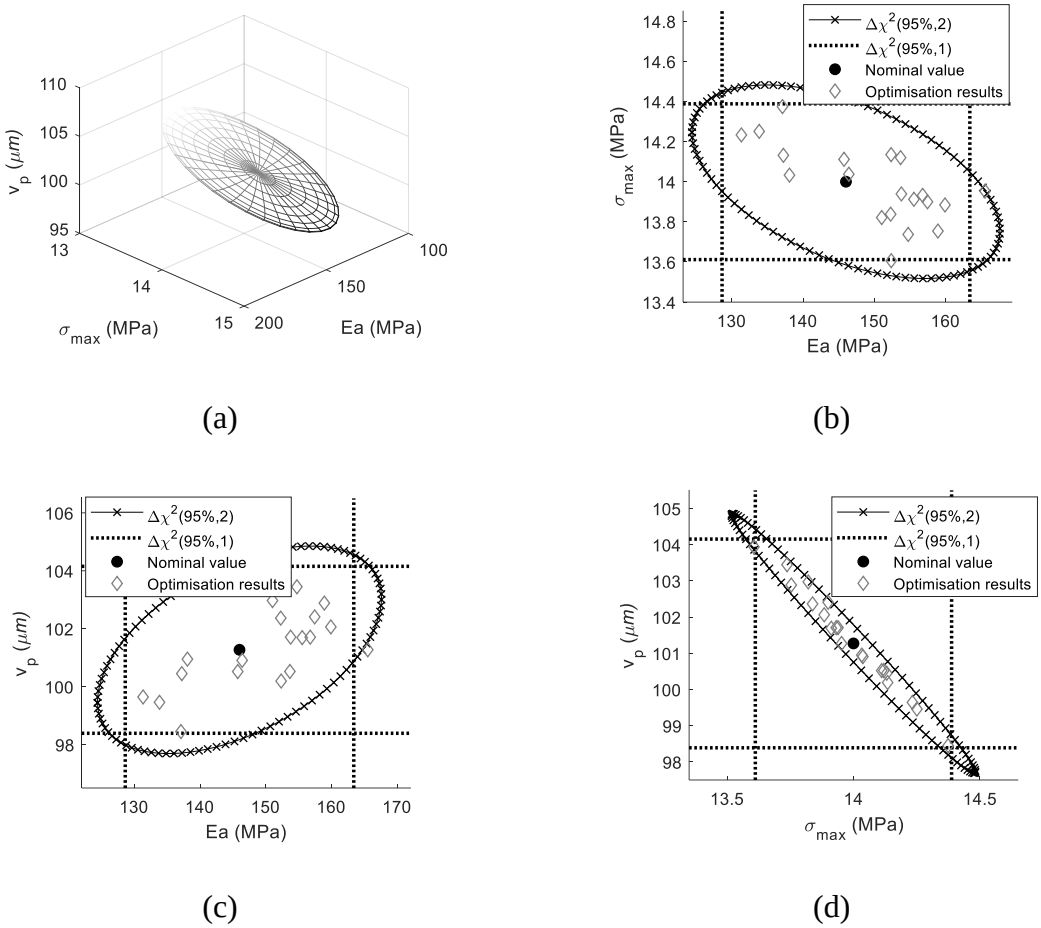

Figure 8: Confidence regions at 95% for the Force-displacement response: (a) confidence ellipsoid; (b) confidence ellipse for E_a and σ_{max}; (c) confidence ellipse for E_a and v_p; (b) confidence ellipse for σ_{max} and v_p

The coupling between the parameters (i.e. E_a/σ_{max}, E_a/δ_p, σ_{max}/δ_p) can also be obtained with the correlation matrix (eq 6), in the force-displacement case it gives:

$$corr = \begin{bmatrix} 1 & -0.51 & 0.50 \\ -0.51 & 1 & -0.99 \\ 0.5 & -0.99 & 1 \end{bmatrix} \qquad \text{(eq 8)}$$

The correlation matrix indicates that the variation of the maximal stress and displacement jump at propagation are so highly correlated that the variation of one can be quasi entirely compensated by the other one, posing the problem of evaluation reliability. This implicates that the parameters triplet chosen is not well defined for this mechanical response. To

eliminate this constraint, one could want to study the variation of critical energy release rate instead of v_p for instance.

Moreover, the confidence regions and interval should be analysed carefully as the methods uses quadratic approximation when it is not necessarily true. Thus, the real confidence regions might not be regular ellipses and confidence intervals in one dimension might not be symmetric. However, this method enables the easy comparison of the different mechanical responses that can be used to determine the adhesive traction separation law parameters.

5 Comparisons

The analysis procedure presented earlier has been applied to the other mechanical response as well. From this study, an evaluation of the methods can be made from the comparison of the confidence intervals, confidence regions and parameters coupling.

5.1 Confidence intervals and regions

The most straightforward results to analyse are the confidence intervals for each parameter individually. They are symmetric and centred around the nominal value. Therefore, the comparison between the methods will only be made with the interval radius. The results for every method and every parameter for a 95% confidence interval are summarized in Table 4

Table 4: 95% confidence intervals comparison

Method	**P(Δ)**	**J(θ,δ)**	**Gauges**	**DIC - Deflection**	**DIC - Rotation**
$\boldsymbol{E_a}$ (MPa)	18.70	13.22	10.78	5.29	5.53
$\boldsymbol{\sigma_{max}}$ (MPa)	0.42	0.17	0.55	0.12	0.12
$\boldsymbol{v_p}$ (μm)	3.10	1.21	4.03	1.23	1.15

Overall, it appears that the results obtained using DIC are better than the other methods especially for the determination of the initial modulus where the deflection confidence interval (CI) radius is of 5.3 MPa. For the stress and the displacement jump, the DIC-rotation

dominates once again with radius of 0.12 MPa and 1.15 µm respectively. However, $J(\theta,\delta)$ gives close results with CI radius of 0.17 MPa and 1.21 µm.

Another insight on the differences between the methods is given by the correlation matrix (Table 5). Indeed, for each method parameters coupling appears to be different but follow the same tendencies. The couple σ_{max}/δ_p appears to be strongly correlated for every methods. This implies that during the minimisation their correct value might not have been found accurately as a small variation of one compensate the deviation of the other. The two other couples are moderately correlated. The use of DIC-deflection seems to ensure a low correlation between the modulus and both σ_{max} and δ_p.

Table 5: Correlation between the parameters couple

Method	P(Δ)	J(θ,δ)	Gauges	DIC - Deflection	DIC - Rotation
$\boldsymbol{E_a/\sigma_{max}}$	-0.510	-0.639	-0.751	-0.149	-0.551
$\boldsymbol{E_a/\delta_p}$	0.500	0.635	-0.747	0.160	0.476
$\boldsymbol{\sigma_{max}/\delta_p}$	-0.990	-0.996	-0.998	-0.980	-0.975

The visual analysis of the confidence ellipses given by the projection of the ellipsoid on two dimensions planes gives complementary information (Figure 9). The smallest interval regions are obtained for both DIC methods again.

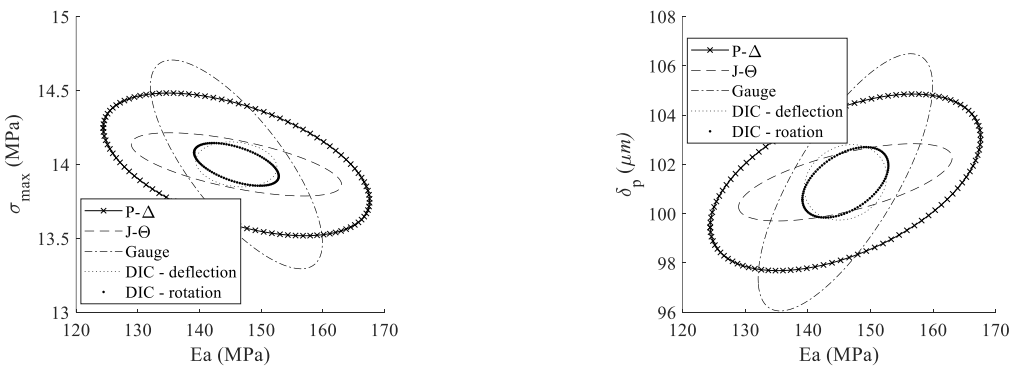

(a) (b)

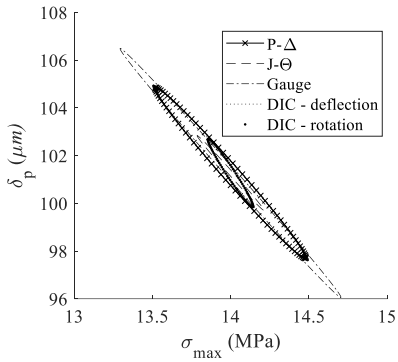

(c)

Figure 9: Comparison of two-dimensions 95% interval regions comparison: (a) Modulus and maximal stress plane; (b) Modulus and displacement jump at propagation plane; (c) Maximal stress Modulus and displacement jump at propagation plane.

The ellipsoid volume analysis gives the overall confidence intervals as it reflects the tightness of the confidence intervals in three dimensions. A small volume indicates a better estimation. Table 6 shows that the DIC in rotation gives the smallest volume.

Table 6: 95% confidence ellipsoid volume

	P(Δ)	**J(θ,δ)**	**Gauge**	**DIC - deflection**	**DIC - rotation**
Volume	35.71	2.06	11.74	1.86	1.52

5.2 TSL confidence envelop

From the three dimensions confidence volume, it is possible to determine the TSL that are on the verge of the 95% confidence surface. Each parameter triplet, which is on the ellipsoid surface, is used to generate the CZM envelope illustrated in Figure 10(a,c,e,g,i). From these envelops the associated mechanical field envelop can be computed (Figure 10(b,d,f,h,j)). It appears that even for the broader envelops the impact on the computed mechanical fields seems to be negligible. That is to say that if the motivation of the CZM identification is only the simulation of the mechanical fields response, then each of these methods gives correct

results. However, if the TSL parameters are used to simulate the behaviour of other kind of assemblies that can have a failure behaviour more sensitive to them than to G_c, then better results will be obtained for DIC or J(θ,δ) methods as the parameters identified are closer to the real nominal response.

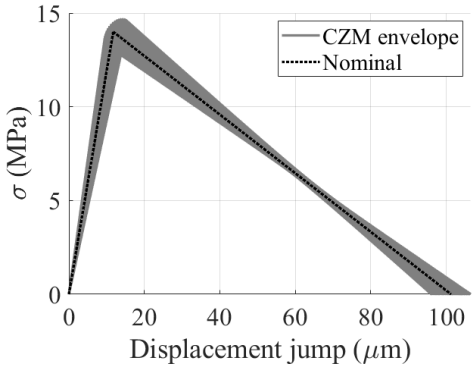

(a)

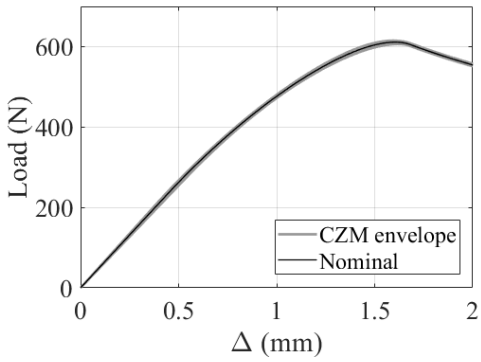

(b)

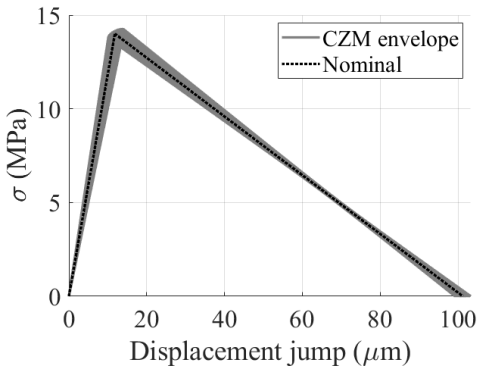

(c)

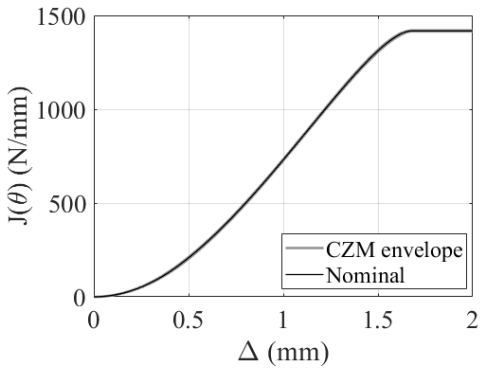

(d)

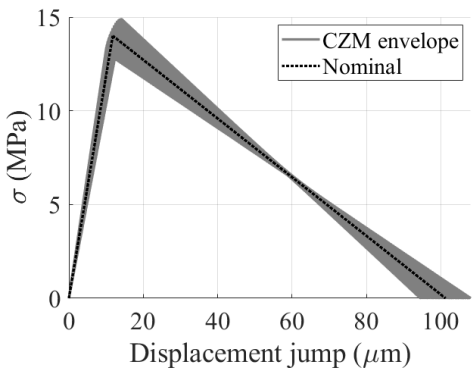

(e)

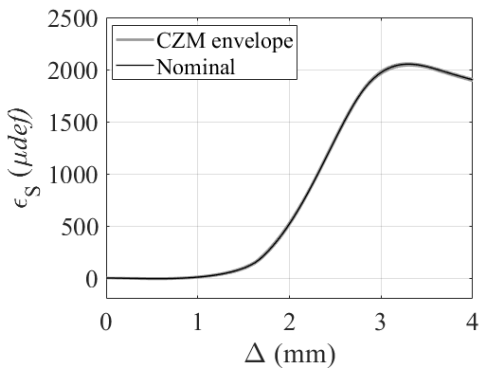

(f)

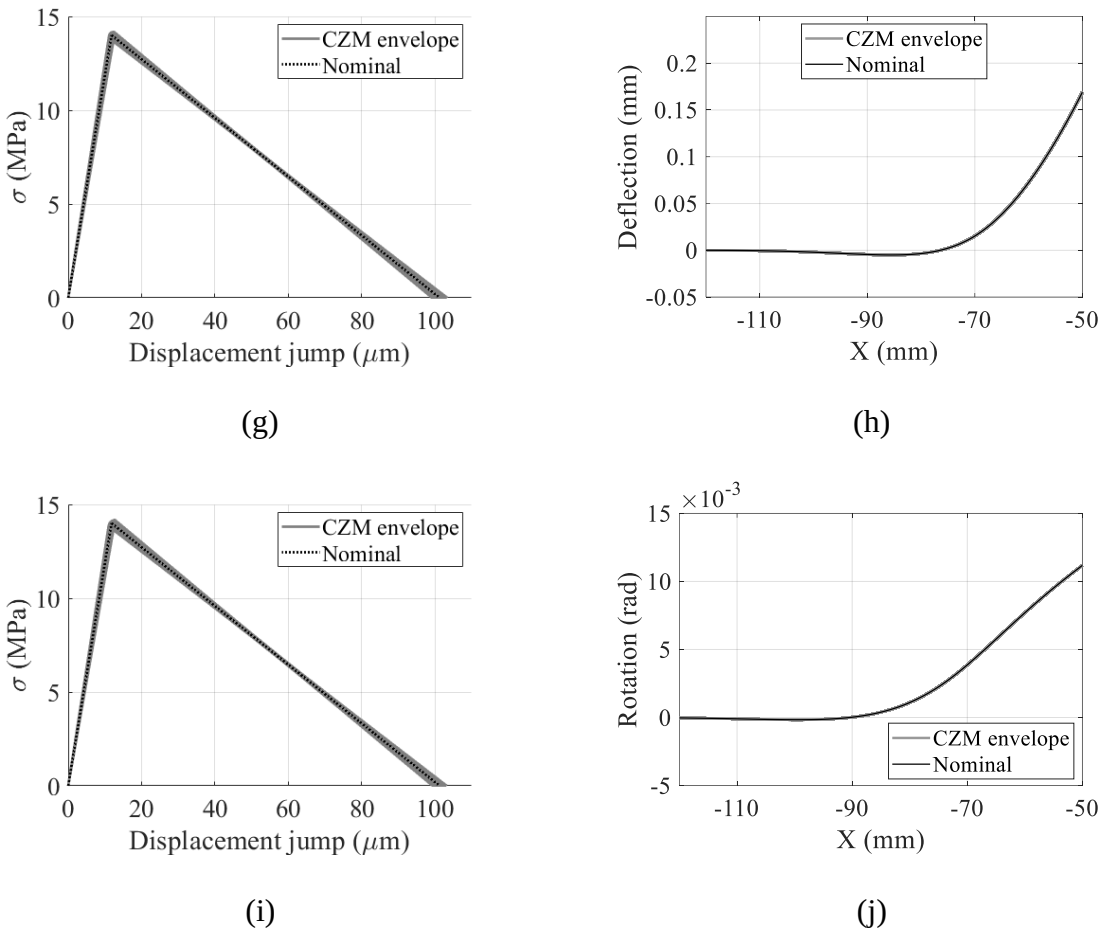

Figure 10: Traction separation law envelope for 95% confidence regions: (a) P(Δ); (b) J(θ,δ); (c) Gauges; (d) DIC – deflection; (e) DIC – rotation

Moreover, as the DCB test was designed to determine the critical energy release rate G_c in mode I**,** another verification can be done using its evaluation for the 95% confidence ellipsoid surface. In Table 7, it appears that all methods except the gauges give a prediction with less than 0.05% variation from the nominal value, which is equal to 1.41780 N/mm.

Table 7: Critical energy release rate evaluation for the 95% confidence volume

	P(Δ)	**J(θ,δ)**	**Gauge**	**DIC - deflection**	**DIC - rotation**
$\boldsymbol{G_{c,moy}}$	1.41708	1.41766	1.41622	1.41773	1.41775
std	0.0071	0.0018	0.0049	0.0051	0.0048

5.3 TSL application to a SLJ

In order to highlight the importance of the TSL parameter estimation, a semi analytical model developed by Paroissien et al. has been used to simulate the force-versus displacement results of a single-lap-joint test [14] [27]. The test geometry presented in Table 8 has been chosen in order to obtain a failure caused predominantly by peeling rather than shear [28]. According to Martin et al. for this test case, the mode mixity is simply managed by setting the same TS law in mode II than in mode I. Moreover, the numerical results provided come from converged model in terms of element density per characteristic length [29]. Table 8 presents the geometric and material characteristics of the SLJ test.

To evaluate the impact of the TSL, the superior and inferior boundaries of the P(Δ) CZM envelope were tested (Figure 11(a)). As illustrated in Figure 11(b), for a similar shear behaviour but different TSL in mode I, the differences obtained are quite important. It appears that there is a variation of 2000N in maximum load. This stresses out the importance of a reliable estimation of the TSL parameters when carrying out the identification on a different mechanical test.

Table 8: SLJ specimen geometric and material characteristics

Adherends		**Adhesive**	
Length outside the overlap (mm)	50	G_a (MPa)	50
Overlap length (mm)	50	e_a(mm)	0.247
Initial crack length (mm)	50	E_a^{inf} (MPa)	163
Thickness (mm)	10	σ_{max}^{inf}(MPa)	13.3
Width (mm)	25	G_c^{inf} (N/mm)	1.4167
Young modulus (GPa)	210	E_a^{sup} (MPa)	129

Poisson ratio (-)	0.3	σ_{max}^{sup}(MPa)	14.7
		G_c^{sup} (N/mm)	1.4137

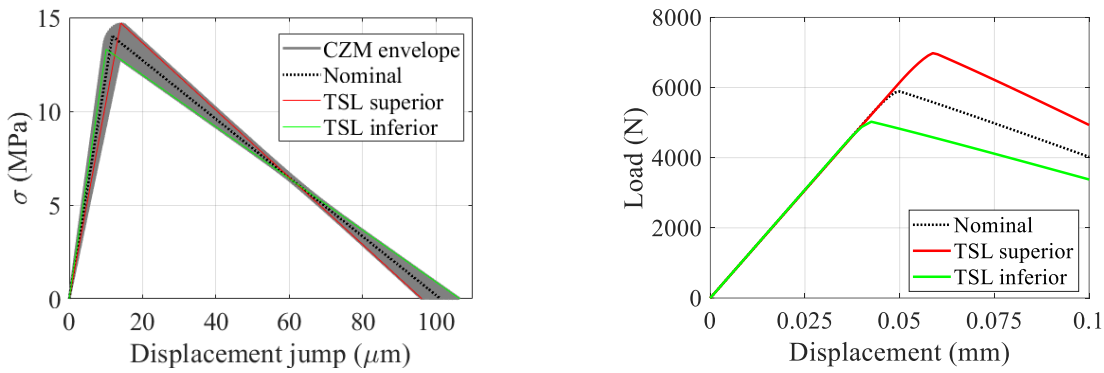

(a) (b)

Figure 11: (a) TSL envelope for the force-displacement; (b) Force versus displacement results of a SLJ

Conclusion

The DCB test is widely used to identify the adhesive behaviour. However, the identification of the correct TSL parameters from this test can be challenging because its mechanical response appears not to be very sensitive. However, a reliable estimation of the mode I TSL is needed when simulating other mechanical tests that are subjected to more complex solicitations. A virtual test campaign has then been carried out in order to determine if one or several of its mechanical fields enables a more accurate identification of the triangular TSL parameter. To do so, the χ^2 minimization has been applied on synthetic experimental data. Its analysis enables the identification of the parameters confidence domains, as well as their coupling. It showed that in order to determine the parameters of an arbitrarily chosen TSL shape (triangular) with an inverse method, the smallest confidence regions are given by digital image correlation. The overall parameter estimation is better when measuring the

adherends' rotation but the analysis of the deflection ensures a smaller coupling between the parameters. The slight augmentation of the confidence volume might be compensated by a more accurate prediction of the parameters. This is to be expected has DIC gives access to more data throughout the test. However, as the use of DIC needs a high investment in equipment, the parameters can also be obtained using the J(θ,δ) method. It gives similarly good results but its analysis needs to be done more carefully as its theoretical background is limiting.

Acknowledgment

As part of the collaborative project S3PAC (FUI 21), this work was co-funded by BPI France, the Occitanie region and the Nouvelle Aquitaine region.

References

[1] A. Cornec, I. Scheider and K.-H. Schwalbe, "On the practical application of the cohesive model," *Engineering fracture mechanics,* vol. 70, pp. 1963-1987, 2003.

[2] J. Chen, "Predicting progressive delamination of stiffened fibre-composite panel and repaired sandwich panel by decohesion models," *Journal of Thermoplastic Composite Materials,* vol. 15, pp. 429-442, 2002.

[3] N. Chandra, H. Li, C. Shet and H. Ghonem, "Some issues in the application of cohesive zone models for metal--ceramic interfaces," *International Journal of Solids and Structures,* vol. 39, pp. 2827-2855, 2002.

[4] L. Škec, "Identification of parameters of a bi-linear cohesive-zone model using analytical solutions for mode-I delamination," *Engineering Fracture Mechanics,* vol. 214, pp. 558-577, 2019.

[5] C. D. M. Liljedahl, A. D. Crocombe, M. A. Wahab and I. A. Ashcroft, "Modelling the environmental degradation of adhesively bonded aluminium and composite joints using a CZM approach," *International Journal of Adhesion and Adhesives,* vol. 27, pp. 505-518, 2007.

[6] M. S. Kafkalidis, M. D. Thouless, Q. D. Yang and S. M. Ward, "Deformation and fracture of adhesive layers constrained by plastically-deforming adherends," *Journal of Adhesion Science and Technology,* vol. 14, pp. 1593-1607, 2000.

[7] M. Alfano, F. Furgiuele, A. Leonardi, C. Maletta and G. H. Paulino, "Mode I fracture of adhesive joints using tailored cohesive zone models," *International journal of fracture,* vol. 157, pp. 193-204, 2009.

[8] R. D. S. G. Campilho, M. D. Banea, J. A. B. P. Neto and L. F. M. Silva, "Modelling

adhesive joints with cohesive zone models: effect of the cohesive law shape of the adhesive layer," *International Journal of Adhesion and Adhesives,* vol. 44, pp. 48-56, 2013.

[9] S. H. Song, G. H. Paulino and W. G. Buttlar, "Influence of the cohesive zone model shape parameter on asphalt concrete fracture behavior," in *AIP Conference Proceedings,* 2008.

[10] B. F. Sørensen, A. Horsewell, O. Jørgensen, A. N. Kumar and P. Engbæk, "Fracture resistance measurement method for in situ observation of crack mechanisms," *Journal of the American Ceramic Society,* vol. 81, pp. 661-669, 1998.

[11] B. F. Sørensen and T. K. Jacobsen, "Determination of cohesive laws by the J integral approach," *Engineering fracture mechanics,* vol. 70, pp. 1841-1858, 2003.

[12] T. Andersson and U. Stigh, "The stress--elongation relation for an adhesive layer loaded in peel using equilibrium of energetic forces," *International Journal of Solids and Structures,* vol. 41, pp. 413-434, 2004.

[13] B. Shen and G. H. Paulino, "Direct extraction of cohesive fracture properties from digital image correlation: a hybrid inverse technique," *Experimental Mechanics,* vol. 51, pp. 143-163, 2011.

[14] G. Lelias, E. Paroissien, F. Lachaud, J. Morlier, S. Schwartz and C. Gavoille, "An extended semi-analytical formulation for fast and reliable mode I/II stress analysis of adhesively bonded joints," *International Journal of Solids and Structures,* vol. 62, pp. 18-38, 2015.

[15] M. Alfano, G. Lubineau and G. H. Paulino, "Global sensitivity analysis in the identification of cohesive models using full-field kinematic data," *International Journal of Solids and Structures,* vol. 55, pp. 66-78, 2015.

[16] B. Blaysat, J. P. M. Hoefnagels, G. Lubineau, M. Alfano and M. G. D. Geers, "Interface debonding characterization by image correlation integrated with double cantilever beam kinematics," *International Journal of Solids and Structures,* vol. 55, pp. 79-91, 2015.

[17] D. Sans, J. Renart, J. Costa, N. Gascons and J. A. Mayugo, "Assessment of the influence of the crack monitoring method in interlaminar fatigue tests using fiber Bragg grating sensors," *Composites Science and Technology,* vol. 84, pp. 44-50, 2013.

[18] J. Jumel, M. K. Budzik, N. B. Salem and M. E. R. Shanahan, "Instrumented End Notched Flexure--Crack propagation and process zone monitoring. Part I: Modelling and analysis," *International Journal of Solids and Structures,* vol. 50, pp. 297-309, 2013.

[19] J. Jumel, N. B. Salem, M. K. Budzik and M. E. R. Shanahan, "Measurement of interface cohesive stresses and strains evolutions with combined mixed mode crack propagation test and Backface Strain Monitoring measurements," *International Journal of Solids and Structures,* vol. 52, pp. 33-44, 2015.

[20] A. Jaillon, J. Jumel, E. Paroissine and F. Lachaud, "Mode I Cohesive Zone Model Parameters Identification and Comparison of Measurement Techniques for Robustness to the Law Shape Evaluation," *Journal of adhesion,* p. Accepted, 2019.

[21] H. Haddadi and S. Belhabib, "Use of rigid-body motion for the investigation and estimation of the measurement errors related to digital image correlation technique," *Optics and Lasers in Engineering,* vol. 46, pp. 185-196, 2008.

[22] S. Marsili-Libelli, S. Guerrizio and N. Checchi, "Confidence regions of estimated parameters for ecological systems," *Ecological Modelling,* vol. 165, pp. 127-146, 2003.

[23] S. Hartmann and R. R. Gilbert, "Identifiability of material parameters in solid mechanics," *Archive of Applied Mechanics,* vol. 88, pp. 3-26, 2018.

[24] S. Mostovoy and E. J. Ripling, "Fracture toughness of an epoxy system," *Journal of*

Applied Polymer Science, vol. 10, pp. 1351-1371, 1966.

[25] J. D. Gunderson, J. F. Brueck and A. J. Paris, "Alternative test method for interlaminar fracture toughness of composites," *International Journal of Fracture,* vol. 143, pp. 273-276, 2007.

[26] T. Andersson and A. Biel, "On the effective constitutive properties of a thin adhesive layer loaded in peel," *International Journal of Fracture,* vol. 141, pp. 227-246, 2006.

[27] E. Paroissien, F. Lachaud, F. M. da Silva and Lucas and S. Seddiki, "A comparison between macro-element and finite element solutions for the stress analysis of functionally graded single-lap joints," *Composite Structures,* vol. 215, pp. 331-350, 2019.

[28] L. J. Hart-Smith, "Adhesive-Bonded Single-Lap Joints.[analytical solutions for static load carrying capacity]," 1973.

[29] E. Martin, T. Vandellos, D. Leguillon and N. Carrère, "Initiation of edge debonding: coupled criterion versus cohesive zone model," *International Journal of Fracture,* vol. 199, pp. 157-168, 2016.